Research Square

Preprints are preliminary reports that have not undergone peer review.
They should not be considered conclusive, used to inform clinical practice,
or referenced by the media as validated information.

A novel monomer of Elephantopus mollis H.B.K., EM-6, inhibits the proliferation of Huh-7 cells by blocking autophagic flux and activating the ROS/MAPK pathway

Changyan Hou
The Affiliated Shunde Hospital of Jinan University
Ruoxuan Lou
Jinan University
Zhihui Wu
Jinan University
Jingjing Tang
the First Affiliated Hospital of Jinan University
Na Zhao
Jinan University
Xinwen Xu
the First Affiliated Hospital of Jinan University
Junzhen Zhou
the First Affiliated Hospital of Jinan University
Peiqian Xiong
Jinan University
Qiang Li
the First Affiliated Hospital of Jinan University
Qing Zhang
the First Affiliated Hospital of Jinan University
Yue Jiang
The Affiliated Shunde Hospital of Jinan University
Jianwei Jiang
jjw703@jnu.edu.cn

Jinan University

Research Article

Keywords: Elephantopus mollis H.B.K., Autophagy flux inhibition, ROS, MAPK, Apoptosis

Posted Date: March 7th, 2024

DOI: https://doi.org/10.21203/rs.3.rs-4014050/v1

License: This work is licensed under a Creative Commons Attribution 4.0 International License.
Read Full License

Additional Declarations: No competing interests reported.

Abstract

Purpose

Primary liver disease is one of the major health problems in the world, and the prognosis of liver cancer is very poor. Liver cancer cells develop strong resistance to clinical chemotherapy drugs, leading to repeated liver cancer.

Materials and Methods

RNA-sequence was applied to related signal pathways that significantly altered. Flow cytometry and Western blot were performed to detect the changes of cell cycle, apoptosis and MAPK pathways. Immunofluorescence and flow cytometry were used to detect changes in cell mitochondrial membrane potential and intracellular ROS levels. Western blot, immunofluorescence, qRT-PCR and mCherry-GFP-LC3 were used to detect the effect of autophagy. Western blot and qRT-PCR were utilized to detect the effect of ER Stress.

Results

EM-6 is a novel monomer purified from Elephantopus mollis H.B.K. Mechanistically, compared with cisplatin (CDDP), EM-6 significantly inhibited the proliferation of human hepatocellular cancer cell lines and had less toxicity to human normal epithelial cells. EM-6 can induce mitochondrial membrane potential disruption, which leads to the accumulation of ROS, S-phase arrest and activation of the IRE1α-ASK1-JNK/p38 pathway to promote apoptosis in Huh-7 cells. In addition, EM-6 blocked protective autophagy by inhibiting the initiation of autophagy, and inhibiting the formation of autophagolysosomes triggered Huh-7 cell apoptosis.

Conclusion

Taken together, our findings suggest that EM-6 activates mitochondrial apoptosis through the ROS/MAPK pathway and promotes the activation of ER stress and the inhibition of autophagic flux to exacerbate apoptosis. These studies demonstrated the promising future of EM-6 in the clinical treatment of hepatocellular cancer.

1. Introduction

Primary liver cancer (PLC) is the fourth most common malignant tumor and represents approximately 4% of all new cancer cases diagnosed worldwide. Currently, liver cancer remains a global public health challenge, and its incidence has been increasing worldwide [1]. By 2025, more than one million people will be affected each year [2]. As the main type of primary liver cancer, HCC accounts for more than 80%-90%

of PLCs. Most patients with HCC have a poor prognosis, which results in small differences in the incidence and mortality of liver cancer worldwide [3]. Moreover, most patients are diagnosed with HCC at an advanced stage, which is not suitable for surgery. The postoperative recurrence rate within 2 years is still as high as 50% in a small number of people [4]. Chemotherapy is a common treatment method for HCC. Sorafenib, lenvatinib, which is noninferior to sorafenib, and regorafenib increase survival and are the standard treatments in advanced hepatocellular carcinoma [5]. However, these agents often cause severe toxicity and side effects in the body, and hepatocellular cancer cells are easily resistant to chemical drugs. In this regard, finding a new drug with high efficiency and less toxicity is highly important.

Elephantopus mollis (Asteraceae) is a popular perennial medicinal plant that has been used medicinally in China for at least 500 years. It is most commonly used for its anti-inflammatory, antipyretic, diuretic, cough and pain relief effects [6]; its antiviral, antitumor and liver protection effects have been proven [7]. Recently, two sesquiterpene lactones, isodeoxyelephantin (ESI) and deoxyelephantin (ESD), have been shown to exert antitumor effects on various malignancies [8]. Shao et al. reported that ROS accumulation and ASK1/JNK signaling pathway activation by EM23, a natural sesquiterpene lactone family member isolated from Elephantopus mollis, are critical for the induction of apoptosis in human cervical cancer (CaSki and SiHa) cell lines [9].

The mitogen-activated protein kinase (MAPK) family comprises serine/threonine protein kinases. Activated MAPK can transmit extracellular signals to regulate cell growth, proliferation, differentiation, migration, and apoptosis [10]. The main members of the MAPK signaling pathway have gradually become new targets for antitumor research [11–12]. At present, the known MAPKs mainly include p38 MAPK, extracellular signal-regulated kinase (ERK), and c-Jun NH2-terminal kinase (JNK) [13]; they are activated by complex and diverse higher-level kinases, which ultimately drive specific target genes to express corresponding transcription factors so that cells can adapt to different external stimuli. Liu et al. demonstrated that CDCA suppresses AML progression by synergistically promoting LD accumulation and lipid peroxidation via the ROS/p38 MAPK/DGAT1 pathway through mitochondrial dysfunction in leukemia cells and inhibition of M2 macrophage polarization [14]. In our previous studies, PP-22, a Paris polyphylla monomer, was shown to induce autophagy and apoptosis in CNE-2 nasopharyngeal carcinoma cells by activating p38 signaling and endoplasmic reticulum stress [15]. However, the effect of EM-6 on MAPK family activity in HCC is unknown.

In our previous study, we isolated 25 sesquiterpene lactone monomers from *Elephantopus mollis* H.B.K. and found that EM-6 has excellent antitumor effects. Preliminary studies have shown that EM-6 has good inhibitory effects on HepG2, MDA-MB-231 and MDA-MB-468 cells. In this study, we demonstrated that EM-6 induces mitochondrial membrane potential damage and results in ROS-mediated S phase arrest and apoptosis. The compound affected the ROS/MAPK pathway to induce Huh-7 cell apoptosis. Moreover, we showed that EM-6 blocked the completion of autophagy by inhibiting the initiation of autophagy and the formation of autophagolysosomes. EM-6 also activated ER stress and induced cell

apoptosis through the IRE1α-ASK1-JNK/p38 pathway in Huh-7 cells. These data suggested that EM-6 is a potential drug with promising antitumor effects for the treatment of HCC.

2. Materials and Methods

Chemicals and reagents

EM-6 was donated by Professor Wang Guocai, School of Pharmacy, Jinan University. The purity of EM-6 was ≥ 95%, as determined by high-performance liquid chromatography. EM-6 was dissolved in dimethyl sulfoxide (DMSO), aliquoted and stored at -80°C.

Antibodies PARP(#9542), Caspase-9(#9502), Caspase-3(#9668), Bax(#5023), Bcl-xL(#2764), Bcl-2(#15071), Mcl-1(#5453), Bip(#3183), PERK(#3192), p-PERK(#3179), IRE1α(#3294), ATF-6(#65880), XBP-1 s(#12782), CHOP(#2895), ASK1(#3762), p-ASK1(Ser967) (#3764), Atg5(#12994), Beclin-1(#3495), p62(#88588), LC3(#12741), Cathepsin D(#2284), CyclinA2(#4656), CyclinD1(#2978), CDK2(#2546), p27(#3698), p21(#2947), p38MAPK(#8690), p-p38(#4511), p44/42MAPK (Erk1/2) (#4695), p-p44/42 MAPK (Erk1/2) (#4377),SAPK/JNK(#9252),p-SAPK/JNK(#4668),c-Jun(#9165),p-c-Jun(#9261),β-Actin(#3700), GAPDH(#5174) were purchased from Cell Signaling Technology (Boston, MA). Goat anti-mouse IgG (H + L) (Cat no: SA00014-10) and goat anti-rabbit IgG (H + L) (Cat no: SA00014-9) were purchased from Proteintech.

Cell culture

HepG2, BEL-7402, Huh-7, SMMC-7721, MHCC97-H, LO2 and HBE cells were purchased from the American Type Culture Collection (ATCC). HepG2, Huh-7 and MHCC97-H cells were cultured in high-glucose DMEM containing 10% FBS. BEL-7402, SMMC-7721, LO2 and HBE cells were cultured in RPMI-1640 medium supplemented with 10% FBS. The cells were cultured at 37°C in an atmosphere containing 5% CO2.

Cell viability assay

Cells were seeded into 96-well plates at a density of 5000 cells per well and treated with different concentrations of EM-6 for 48 hours. MTT solution (5 mg/mL) was added to each well, and the cells were cultured for 4–6 h. The absorbance was subsequently measured at 570 nm by a microplate reader (Bio-Rad Laboratories, Hercules, CA, USA).

EdU staining assay

Cells were seeded into 96-well plates at a density of 5000 cells per well and treated with different concentrations of EM-6 for 24 h. Then, EdU staining assays were performed to detect cell proliferation activity via a KFluor488-EdU detection kit (KeyGEN, Jiangsu, China) according to the manufacturer's instructions.

Colony formation assay

Cells were seeded in 6-well plates at a density of 1000 cells per well and then exposed to different concentrations of EM-6 for 7 days. Then, the cells were fixed with 4% paraformaldehyde for 20 min and stained with 0.5% crystal violet solution (Sigma, USA) for 30 min. After three gentle washes and air drying, the stained colonies were counted and photographed.

Reactive oxygen species detection

Cells were seeded in 6-well plates at a density of 3×10^5 cells per well and then exposed to different concentrations of EM-6 for 24 h. DCFH-DA probes were added, and the mixture was incubated at 37°C for 1 h. The fluorescence intensity of DCF was detected via flow cytometry.

RT—qPCR and RNA sequencing

Total RNA was extracted from isolated cells using TRIzol reagent (Life, CA, USA), and reverse transcription was performed with a HiScript II RT SuperMix for qPCR (+ gDNA wiper) reverse transcription cassette. The qPCR primers (Vazyme Biotech, Nanjing, China) used were purchased from Beijing TSINGKE synthesis, and the primer sequences are shown in Table 1. Total cell RNA was extracted from the cells, after which the cells were sent to BGI for RNA sequencing via the BGISEQ-500 sequencing platform.

Table 1

gene name	Primer sequence	
HSPA5	Forward	5'-CTGTCCAGGCTGGTGTGCTCT-3'
	Reverse	5'-CTTGGTAGGCACCACTGTGTTC-3'
XBP-1 s	Forward	5'-TGCTGAGTCCGCAGCAGGTG-3'
	Reverse	5'-GCTGGCAGGCTCTGGGGAAG-3'
EIF2AK3	Forward	5'-GTCCCAAGGCTTTGGAATCTGTC-3'
	Reverse	5'- CCTACCAAGACAGGAGTTCTGG-3'
ERN1	Forward	5'- CGTCCCCAGATTCACTGTCC-3'
	Reverse	5'- GTACGACACCAAAACCCGAG-3'
ATF4	Forward	5'- TTCTCCAGCGACAAGGCTAAGG-3'
	Reverse	5'- CTCCAACATCCAATCTGTCCCG-3'
DDIT3	Forward	5'-ACCAGGAAACGGAAACAG-3'
	Reverse	5'-TCACCATTCGGTCAATCA-3'
SQSTM1	Forward	5'-GACTACGACTTGTGTAGCGTC-3'
	Reverse	5'-AGTGTCCGTGTTTCACCTTCC-3'
ATG5	Forward	5'-TCAGCCACTGCAGAGGTGTTT-3'
	Reverse	5'-GGCTGCAGATGGACAGTTGCA-3'
BECN1	Forward	5'-ACTCAGCTCAACGTCACTGAAA-3'
	Reverse	5'-TCTTGCGGTTCTTTTCCACG-3'
ATG7	Forward	5'-ACCCAG AAGAAGCTGAACGA-3'
	Reverse	5'-CTCATTTGCTGCTTGTTCCA-3'
ATG12	Forward	5 -GATCCGGGGATTTCTTTCACG-3
	Reverse	5 -CAGCAATGTAAGACCAGTCAAGT-3
MAP1LC3B	Forward	5'-ACCCTGAGTCTTCTCTTCAGGT-3'
	Reverse	5'-CAGTCAGGGCCGTTTTCTCA-3'
GAPDH	Forward	5'-AAGAAGGTGGTGAAGCAGG-3'
	Reverse	5'-TTGACAAAGTGGTCGTTGAG-3'

Cell cycle and apoptosis analysis

Propidium iodide (PI) staining was performed to analyze the cell cycle distribution.

Cells were seeded in 6-well plates and exposed to different concentrations of EM-6 for 48 h before they were harvested and fixed with 70% ethanol for 12 h at 4°C. The cells were incubated with the JNK inhibitor SP600125 (20 μM), the p38 inhibitor SB203580 (15 μM), or the ERK inhibitor trametinib (25 μM) (Selleck, USA) for 8 h and with the reactive oxygen species scavenger NAC (5 mM) for 1 h. Cells were stained according to the instructions of the Cell Cycle Analysis Kit (KeyGEN, Jiangsu, China). Apoptosis was detected according to the instructions of the Annexin V-FITC/PI Apoptosis Detection Kit (KeyGEN, Jiangsu, China). Flow cytometry was used to detect cell cycle distribution and apoptosis.

Mitochondrial membrane potential

Cells were seeded in 6-well plates at a density of 3×10^5 cells per well and then exposed to different concentrations of EM-6 for 24 h. The mitochondrial proton carrier uncoupler (CCCP) (10 μM) (Selleck, USA) was used as a positive control and was pretreated for 20 min. Then, 1 mL of JC-1 staining solution (KeyGEN, Jiangsu, China) was added, and the mixture was incubated at 37°C for 15 min. An inverted fluorescence microscope (LeciaDMi8, Germany) was used to determine the ratio of the fluorescence intensity.

Active Caspase-3 detection

Cells were seeded in 6-well plates at a density of 3.0×10^5 cells per well and exposed to different concentrations of EM-6 for 48 h. The JNK inhibitor SP600125 (20 μM), the p38 inhibitor SB203580 (15 μM) and the ERK inhibitor trametinib (25 μM) were used to pretreat the cells for 8 h, and the reactive oxygen species scavenger NAC (5 mM) was used for 1 h. The cells were stained according to the instructions of the FITC Active Caspase 3 Apoptosis Kit (BD, USA). A high-sensitivity intelligent flow analyzer (FACS VERSE; BD, USA) was used for detection.

Immunofluorescence assay

Cells were seeded in 12-well plates at a density of 1.5×10^5 cells per well and exposed to different concentrations of EM-6 for 24 h. The cells were treated with 200 μL of 4% paraformaldehyde (YuanyeBio, Shanghai, China) for 10 min and 0.1% Triton X-100 (Solarbio, Beijing, China) for another 10 min and then incubated with 10% goat serum (Boster, Wuhan, China) for 1 h at 37°C. The cells were incubated with a p62 primary antibody (ABclonal, Wuhan, China) overnight at 4°C. After being washed with 1×phosphate buffered saline containing 2% Tween 20 (Solarbio, Beijing, China), the cells were incubated with the corresponding secondary antibody for 1 h at room temperature. The cells were then sealed with 100 μL of DAPI (KeyGEN, Jiangsu, China) for 10 min. An inverted fluorescence microscope (LeciaDMi8, Germany) was used to determine the ratio of the fluorescence intensity.

mCherry-GFP-LC3 detection

The cells were seeded in 6 cm petri dishes at a density of 5×10^5 cells per well, exposed to 50 μL of polybrene (4 μg/μL) (Solarbio, Beijing, China) for 24 h, and subsequently sieved with puromycin (5 μg/μL) (Solarbio, Beijing, China) for 4 days. The virus-infected cells were seeded into Petri dishes and treated with EM-6 (4 μM) for 24 h. Rapamycin (100 nM) (Beyotime, Shanghai, Beijing) was used to pretreat the cells for 4 h, and bafilomycin A1 (100 nM) (Baf A1) (Selleck, USA) was used to pretreat the cells for 8 h. Then, Hoechst 33342 was added for 15 min. A confocal laser scanning microscope (Lecia TCS SP8, Germany) was used to observe autophagosomes and autolysosomes.

Western blot

The protein concentrations were determined with a BCA kit (Sangon, Shanghai, China). The protein samples were separated via SDS—PAGE and transferred to 0.22 μm PVDF membranes (Merck, Germany). After blocking with 5% skim milk for 1 h, the membranes were incubated with primary antibody overnight at 4°C followed by secondary antibody for 1 h at room temperature. The immunoreactive bands were visualized with a Tanon 5200 imaging system (Tanon, Shanghai, China).

Statistical analysis

All the data are presented as the mean ± standard error of the mean (SEM). Student's t test and one-way ANOVA were performed to analyze the significance of the difference between two groups or among multiple groups, respectively. The statistical analysis was performed using SPSS 20 (SPSS software, IBM, USA) and GraphPad Prism 7.0 (GraphPad software, San Diego, CA, USA). The band intensity was quantified with ImageJ software. P values < 0.05 were considered to indicate statistical significance.

3. Results

3.1 EM-6 inhibited the proliferation of Huh-7 cells

EM-6 is a monomeric sesquiterpene lactone extracted from *Elephantopus mollis* H.B.K., and its chemical structure is depicted in Fig. 1G. MTT assays showed that EM-6 exhibited antiproliferative activity against human hepatocellular cancer cells but had little cytotoxic effect on human normal epithelial cells. The IC50s for human liver epithelial LO2 cells and bronchial epithelial HBE cells were greater than 100 μM (Fig. 1A, B).

According to the MTT results, Huh-7 cells were used in the following research. Compared with cisplatin (CDDP), the conventional chemical drug for HCC, EM-6 had a stronger inhibitory effect on survival (Fig. 1C). EdU and colony formation assays further confirmed the inhibitory effect of EM-6 on proliferation (Fig. 1D, E). The above results showed that EM-6 inhibited the proliferation of Huh-7 cells.

RNA-seq was used to detect changes in physiological processes and signaling pathways in Huh-7 cells after treatment with EM-6. GO function and Kyoto Encyclopedia of Genes and Genomes (KEGG)

enrichment analyses revealed that cell cycle, autophagy and apoptosis were significantly activated (Fig. 1F).

3.2 EM-6 induced S-phase arrest and apoptosis in Huh-7 cells

Apoptosis, also referred to as programmed cell death, is a fundamental process required for morphogenetic homeostasis during early development and in pathophysiological conditions at any stage during an individual's life [16]. Considering the RNA-seq results, the cell cycle and apoptosis were investigated in Huh-7 cells (Fig. 1F). The proportion of Huh-7 cells in S phase significantly increased (Fig. 2A). Western blot analysis showed that the expression of the S phase arrest-related proteins Cyclin A2, CDK2, p27 and p21 significantly increased, while that of Cyclin D1 decreased (Fig. 2C). Taken together, these findings showed that EM-6 could induce S-phase arrest in Huh-7 cells.

Annexin V-FITC and PI double staining was performed to detect the percentage of apoptotic Huh-7 cells. The proportion of apoptotic cells increased in a dose-dependent manner, and the percentage of apoptotic cells increased from 2.83–49.83% after 48 h (Fig. 2B). Western blot analysis revealed that the antiapoptotic proteins Bcl-2, Bcl-xl and Mcl-1 decreased, while the levels of cleaved PARP and the proapoptotic protein Bax increased (Fig. 2D). The percentage of FITC-cl-Caspase-3-positive cells increased from 0.05–35.84% after 48 h (Fig. 2E). The above results showed that EM-6 could induce apoptosis in Huh-7 cells.

3.3 EM-6 induced a decrease in the mitochondrial membrane potential and accumulation of ROS

Mitochondria play a central role in apoptotic cell death. The sequencing results were analyzed by Gene Ontology (GO) functional enrichment, which revealed that EM-6 treatment significantly altered the oxidation–reduction and apoptotic processes in Huh-7 cells (Fig. 3A).

The accumulation of reactive oxygen species (ROS) can cause mitochondrial membrane disorders to induce cell death [17]. Mitochondria are the main source of ROS; therefore, we used the JC-1 probe to detect the effect of EM-6 on the mitochondrial membrane potential (MMP). When the ratio of green to red fluorescence intensity gradually increased, the MMP of the Huh-7 cells decreased (Fig. 3B).

EM-6 increased the level of ROS in a dose-dependent manner, and this effect was reversed by NAC (5 mM) (Fig. 3C, D). The above results indicated that EM-6 could reduce the mitochondrial membrane potential and induce the accumulation of ROS.

3.4 EM-6 induced S-phase arrest and apoptosis through the accumulation of ROS

Increased oxidative damage and enhanced ROS-dependent death signaling can also effectively prevent some steps in tumorigenesis [18]. We further investigated whether EM-6 induces ROS accumulation,

thereby activating cells to develop mitochondria-dominated endogenous apoptosis pathways as well as S-phase cycle arrest. We used the ROS inhibitor NAC in combination with EM-6. The S phase fraction was reduced in the NAC combination group (Fig. 4A). Moreover, Western blot analysis showed that NAC significantly decreased the levels of Cyclin A2, CDK2, p27 and p21, while the level of Cyclin D1 increased (Fig. 4B). In addition, colony formation and MTT assays demonstrated that NAC reversed the inhibitory effect of EM-6 on proliferation (Fig. 4C, D).

The percentage of apoptotic Huh-7 cells decreased from 54.66–3.25% after pretreatment with NAC (Fig. 4E). Moreover, the levels of Bax and cleaved PARP were decreased, while those of Bcl-2, Caspase-9, Caspase-3 and PARP were significantly elevated (Fig. 4F). Moreover, the percentage of FITC-cleaved caspase-3-positive cells decreased from 34.11–0.63% (Fig. 4G). These results indicated that, due to the accumulation of ROS, EM-6 induced S-phase arrest and apoptosis in Huh-7 cells.

3.5 EM-6 activated the MAPK signaling pathway through ROS

We next aimed to determine which pathway was associated with the EM-6-mediated inhibition of HCC cell proliferation. The RNA-seq results analyzed by KEGG showed that EM-6 had a strong impact on the MAPK pathway in Huh-7 cells (Fig. 5A). With increasing concentrations of EM-6, the levels of the MAPK family proteins p-JNK, p-p38 and p-c-Jun significantly increased, while p-ERK had the opposite effect (Fig. 5B).

An increasing number of studies have shown that the accumulation of ROS can activate the MAPK signaling pathway to regulate apoptosis and cell proliferation [19–20]. After pretreatment with NAC, the p-JNK, p-p38 and p-c-Jun levels were significantly decreased (Fig. 5C). The above results showed that EM-6 could activate the MAPK signaling pathway through ROS in Huh-7 cells.

3.6 EM-6 activated the JNK and p38 pathways to induce apoptosis

The present study investigated the relationship between MAPK family proteins and apoptosis in Huh-7 cells. We further detected apoptosis in cells treated with EM-6 in combination with the p38 inhibitor SB203580, the ERK inhibitor trametinib, and the JNK inhibitor SP600125.

Blocking p38 and JNK pathway inhibited the antitumor effect of EM-6, Cleaved-PARP were significantly decreased (Fig. 6B, C), cell viability decreased (Fig. 6D) and apoptosis rate dropped (Fig. 6E). Interestingly, the ERK inhibitor trametinib promoted apoptosis and decreased cell viability (Fig. 6A, D, E). The above results showed that EM-6 induced apoptosis in Huh-7 cells through the activation of the JNK and p38 pathways.

3.7 EM-6 blocked autophagic flux in Huh-7 cells

The RNA-seq results indicated that EM-6 treatment affected the autophagy of Huh-7 cells, as shown in Fig. 1F. The constant activation of autophagy promotes cell apoptosis. Therefore, to determine whether autophagy was activated in Huh-7 cells upon EM-6 treatment, the protein expression levels of autophagy-related proteins were examined via Western blotting. When the expression levels of Beclin1 and Atg7 decreased but those of p62 and LC3 increased, EM-6 induced autophagy (Fig. 7B). Moreover, the mRNA levels of these proteins were detected by RT—qPCR in Huh-7 cells treated with different concentrations of EM-6. Consistent with the Western blotting results, the mRNA levels of autophagy-related genes, such as SQSTM1 and MAP1LC3B, significantly increased with increasing EM-2 concentration (Fig. 7A). We also found that the expression of p62 increased, as determined by immunofluorescence (Fig. 7C). These results revealed that EM-6 blocked autophagic flux. In addition, we found that EM-6 combined with bafilomycin A1 further inhibited the viability of Huh-7 cells (Fig. 7D).

The completion of autophagy depends on the combination of autophagosomes and lysosomes, and the mCherry-GFP-LC3 system is the gold standard for autophagic flux detection. We used rapamycin (Rap, 100 nM) to activate autophagic flux and Baf A1 to block autophagic flux. In the Rap treatment group, the red fluorescence intensity significantly increased, indicating the activation of autophagy. The yellow fluorescent dots represent the inhibition of autophagic flux, and there was a significant increase in the EM-6/rapamycin combination group (Fig. 7E, F, G). These findings demonstrated that EM-6 could block autophagic flux.

3.8 EM-6 activated ER stress-related apoptosis

Studies have reported that the inhibition of autophagic flux promotes ER stress to induce cell apoptosis [21]. The qRT—PCR results showed that the expression of ERN1, HSPA5, EIF2AK3, ATF4, DDIT3, and XBP-1 s was significantly increased in a dose-dependent manner (Fig. 8A), which suggested that EM-6 could activate ER stress in Huh-7 cells.

Furthermore, Bip, IRE1α, XBP-1 s, CHOP and p-PERK increased. Moreover, EM-6 promoted the activation of ASK1 through Ser967 dephosphorylation (Fig. 8B). Studies have reported that the dephosphorylation of Ser-967 is accompanied by increased autokinase activity in ASK1. This change is further accompanied by the increased activity of the JNK and p38 kinases, which are downstream effectors of ASK1 [22]. Therefore, we speculate that EM-6 promotes apoptosis through ER stress and the IRE1α-ASK1-JNK/p38 pathway.

4. Discussion

Hepatocellular cancer (HCC) is the sixth leading cause of cancer incidence and the fourth leading cause of cancer mortality, with approximately 841,000 new cases and 782,000 deaths each year worldwide [23]. More than half of the world's new cases occur in China. Patients are often diagnosed with liver cancer in advanced stages, which contributes to its poor prognosis. Most liver cancer cases involve hepatocellular carcinoma (HCC), for which chemotherapy and immunotherapy are the best therapeutic options. For advanced HCC patients, natural compounds may cause lower organ toxicity and fewer side effects [24].

In recent years, studies have reported that monomers purified from *Elephantopus mollis* H.B.K. exhibit improved antitumor effects with decreased toxicity [25–26]. In our previous study, EM-2 promoted G2/M phase arrest and activated ER stress-related apoptosis by activating the JNK pathway and blocking autophagic flux in Huh-7 cells [26]. We isolated 17 monomers from *Elephantopus mollis* H.B.K. We also observed that EM2, EM3, EM5, EM6, EM7, EM10 and EM12 had better antitumor effects on MDA-MB-231 and MCF-7 cells after treatment with 10 μM monomers for 48 h. Overall, EM6 strongly inhibited the proliferation of human hepatoma cell lines, and we selected EM6 for subsequent experiments.

In this study, we first found that EM-6 exerted a promising antitumor effect, with an IC50 value of 1.83 ± 0.306 μM in Huh-7 cells (Fig. 1A-B). EdU and colony formation assays further demonstrated that EM-6 inhibited proliferation (Fig. 1D-E). The RNA-seq results showed that EM-6 has an impact on the cell cycle, apoptosis and autophagy (Fig. 1F).

The Bcl-2 family of proteins, which are composed of antiapoptotic proteins (Mcl-1, Bcl-2, Bcl-xL, etc.) and proapoptotic proteins (Bax, Bad, etc.), play important roles in the regulation of mitochondrial membrane permeability and membrane potential. When mitochondria are damaged, Bcl-2 family proteins lead to a decrease in the polarity of the transmembrane potential and an increase in membrane permeability. Cytochrome C, Smac and apoptosis-inducing factor (AIF) can be released to activate the caspase-dependent mitochondrial apoptosis pathway. We found that EM-6 can significantly change apoptosis and oxidation–reduction. The JC-1 assay showed that the intensity of the green fluorescence significantly increased. These results suggested that EM-6 caused damage to mitochondria (Fig. 3B), leading to the destruction of the membrane potential and induction of apoptosis.

Mitochondria are the main source of ROS in eukaryotic cells, and an imbalance in redox metabolism often leads to a greater ROS load. Therefore, we further used the ROS detection probe DCFH-DA and found that EM-6 could significantly increase the intracellular ROS level (Fig. 3C) and that the S-phase arrest of Huh-7 cells induced by EM-6 was almost completely reversed after the use of the ROS scavenger NAC (Fig. 4A). These results indicated that EM-6 could induce ROS-induced mitochondrial apoptosis and S-phase arrest.

ROS are important second messengers that can activate the MAPK pathway, which is involved in cell apoptosis [27]. Numerous studies have shown that ROS are upstream of the MAPK signaling pathway and that ROS can activate the MAPK pathway to induce apoptosis and cell cycle arrest [19–20]. We found that pretreatment with the JNK inhibitor SP600125 or the p38 inhibitor SB203580 reduced the expression of cl-PARP and the percentage of apoptotic cells (Fig. 6B-C). EM-6 combined with the ERK inhibitor trametinib increased the level of cl-PARP and the apoptosis rate (Fig. 6A). We suspected that ERK is associated with cell growth and survival. EM-6 inhibited p-ERK and increased Huh-7 cell apoptosis when combined with the ERK inhibitor trametinib.

We also found that EM-6 had a significant effect on autophagy through RNA sequencing (Fig. 1F). We confirmed that EM-6 inhibited the initiation of autophagy and blocked autophagic flux. EM-6 blocked autophagic flux and aggravated endoplasmic reticulum stress. Moreover, EM-6 promoted the activation

of ASK1, which is upstream of p38 and JNK [28], thus inducing various types of apoptosis. Therefore, EM-6 could activate ER stress and induce apoptosis through the IRE1α-ASK1-JNK/p38 pathway.

Conclusion

We demonstrated that EM-6 could significantly inhibit the proliferation of various human hepatocellular cancer cell lines, the smallest of which had an IC_{50} of 1.83 ± 0.306 μM. Moreover, we proved that EM-6 could induce S-phase arrest and activate the ROS/MAPK pathway to induce apoptosis. In addition, EM-6 blocked autophagic flux, induced ER stress and activated the IRE1α-ASK1-JNK/p38 pathway to induce apoptosis in Huh-7 cells. Overall, this study clarified the antitumor effects and molecular mechanisms of EM-6 and provided promising prospects for its future clinical application in treating HCC.

Abbreviations

PBS, Phosphate Buffer Solution; DMSO, Dimethylsulfoxide; IC50, Fifty percent inhibitory concentration; HRP, Horseradish peroxidase; EDTA, Ethylene Diamine Tetraacetic Acid; SPSS, Statistical Package for the Social Science; Caspase, Cysteine aspartate-specific protease; NAC, N-acetyl cysteine ; HPLC, high-performance liquid chromatography; qRT—PCR, quantitative real-time PCR;
TNF, tumor necrosis factor; PLC, primary liver cancer; HCC, hepatocellular cancer; PARP, poly ADP-ribose polymerase; PERK, protein kinase R-like ER kinase; MAPK, mitogen-activated protein kinase; KEGG, Kyoto Encyclopedia of Genes and Genomes.

Declarations

ACKNOWLEDGEMENTS

This research was supported by the First Affiliated Hospital of Jinan University Flagship Specialty Construction Project-General Surgery (No. 711003), the National Natural Science Foundation of China (No. 82074064), and the Natural Science Foundation of Guangdong Province in China (No. 2021A1515012521). Medical Joint Fund Free Application Program in Jinan University (MF220205)

ADDITIONAL INFORMATION

Competing interests: The authors declare no competing interests.The authors have no relevant financial or non-financial interests to disclose.

AUTHOR CONTRIBUTIONS

Zhihui Wu, and Jianwei Jiang contributed to the conception of the study. Changyan Hou contributed to the design and performance of the experiments. Ruoxuan Lou contributed to the data analysis and the writing and submission of the paper. Xinwen Xu, Na Zhao and Junzhen Zhou participated in the discussion. Qiang Li, Jingjing Tang and Qing Zhang contributed to the typesetting and correction of the

paper. Yue Jiang, Junzhen Zhou and Peiqian Xiong contributed to the revision of the article. All the authors read and approved the manuscript.

ETHICS STATEMENT

There were no patients/participants in this study and the study does not required approved by named Institutional review boards or committees.

DATA AVAILABILITY STATEMENT

The data underlying this article are available in PubMed, at https://dx.doi.org/[doi].The data underlying this article are available in the article and in its online supplementary material.

References

1. Villanueva A (2019). Hepatocellular Carcinoma. The New England journal of medicine. 380(15), 1450–1462. doi:10.1056/NEJMra1713263
2. International Agency for Research on Cancer. GLOBOCAN 2018. IARC, 2020
3. Golabi P, Fazel S, Otgonsuren M, Sayiner M, Locklear CT, Younossi ZM (2017). Mortality assessment of patients with hepatocellular carcinoma according to underlying disease and treatment modalities. Medicine. 96(9), e5904. doi:10.1097/MD.0000000000005904
4. Shiffman ML (2018). The next wave of hepatitis C virus: The epidemic of intravenous drug use. Liver international : official journal of the International Association for the Study of the Liver. 38 Suppl 1, 34–39. doi:10.1111/liv.13647
5. Forner A, Reig M, Bruix J (2018). Hepatocellular carcinoma. Lancet (London, England). 391(10127), 1301–1314. doi:10.1016/S0140-6736(18)30010-2
6. Wu ZN, Zhang YB, Chen NH, Li MJ, Li MM, Tang W, Zhuang L, Li YL, Wang GC (2017). Sesquiterpene lactones from Elephantopus mollis and their anti-inflammatory activities. Phytochemistry. 137, 81–86. doi:10.1016/j.phytochem.2017.01.020
7. Ooi KL, Muhammad TS, Tan ML, Sulaiman SF (2011). Cytotoxic, apoptotic and anti-α-glucosidase activities of 3,4-di-O-caffeoyl quinic acid, an antioxidant isolated from the polyphenolic-rich extract of Elephantopus mollis Kunth. Journal of ethnopharmacology. 135(3), 685–695. doi:10.1016/j.jep.2011.04.001
8. Wang Y, Zhang J, Huang ZH, Huang XH, Zheng WB, Yin XF, Li YL, Li B, He QY (2017). Isodeoxyelephantopin induces protective autophagy in lung cancer cells via Nrf2-p62-keap1 feedback loop. Cell death & disease. 8(6), e2876. doi:10.1038/cddis.2017.265
9. Shao FY, Wang S, Li HY, Chen WB, Wang GC, Ma DL, Wong NS, Xiao H, Liu QY, Zhou G X et al (2016). EM23, a natural sesquiterpene lactone, targets thioredoxin reductase to activate JNK and cell death pathways in human cervical cancer cells. Oncotarget. 7(6), 6790–6808. doi:10.18632/oncotarget.6828

10. Sui X, Kong N, Ye L, Han W, Zhou J, Zhang Q, He C, Pan H (2014). p38 and JNK MAPK pathways control the balance of apoptosis and autophagy in response to chemotherapeutic agents. Cancer letters. 344(2), 174–179. doi:10.1016/j.canlet.2013.11.019
11. Guo YJ, Pan WW, Liu SB, Shen ZF, Xu Y, Hu LL (2020). ERK/MAPK signalling pathway and tumorigenesis. Experimental and therapeutic medicine. 19(3), 1997–2007. doi:10.3892/etm.2020.8454
12. Lee S, Rauch J, Kolch W (2020). Targeting MAPK Signaling in Cancer: Mechanisms of Drug Resistance and Sensitivity. International journal of molecular sciences. 21(3), 1102. doi:10.3390/ijms21031102
13. Low HB, Zhang Y (2016) Regulatory roles of MAPK phosphatases in cancer. Immune Netw. 16:85–98. doi:10.4110/in.2016.16.2.85
14. Liu J, Wei Y, Jia W, Can C, Wang R, Yang X, Gu C, Liu F, Ji C, Ma D (2022). Chenodeoxycholic acid suppresses AML progression through promoting lipid peroxidation via ROS/p38 MAPK/DGAT1 pathway and inhibiting M2 macrophage polarization. Redox biology. 56, 102452. doi:10.1016/j.redox.2022.102452
15. Tan GX, Wang XN, Tang YY, Cen WJ, Li ZH, Wang GC, Jiang JW, Wang XC (2019). PP-22 promotes autophagy and apoptosis in the nasopharyngeal carcinoma cell line CNE-2 by inducing endoplasmic reticulum stress, downregulating STAT3 signaling, and modulating the MAPK pathway. Journal of cellular physiology. 234(3), 2618–2630. doi:10.1002/jcp.27076
16. Kashyap D, Garg VK, Goel N (2021). Intrinsic and extrinsic pathways of apoptosis: Role in cancer development and prognosis. Advances in protein chemistry and structural biology. 125, 73–120. doi:10.1016/bs.apcsb.2021.01.003
17. Serrano MC, Feito MJ, González-Mayorga A, Diez-Orejas R, Matesanz M, Portolés MT (2018). Response of macrophages and neural cells in contact with reduced graphene oxide microfibers. Biomaterials science. 6(11), 2987–2997. doi:10.1039/c8bm00902c
18. Cheung EC, Vousden KH (2022). The role of ROS in tumour development and progression. Nature reviews. Cancer. 22(5), 280–297. doi:10.1038/s41568-021-00435-0
19. Yao Y, Cui L, Ye J, Yang G, Lu G, Fang X, Zeng Z, Zhou J (2020). Dioscin facilitates ROS-induced apoptosis via the p38-MAPK/HSP27-mediated pathways in lung squamous cell carcinoma. International journal of biological sciences. 16(15), 2883–2894. doi:10.7150/ijbs.45710
20. Aggarwal V, Tuli HS, Varol A, Thakral F, Yerer MB, Sak K, Varol M, Jain A, Khan MA, Sethi G (2019). Role of Reactive Oxygen Species in Cancer Progression: Molecular Mechanisms and Recent Advancements. Biomolecules. 9(11), 735. doi:10.3390/biom9110735
21. Jia B, Xue Y, Yan X, Li J, Wu Y, Guo R, Zhang J, Zhang L, Li Y, Liu Y et al (2018). Autophagy inhibitor chloroquine induces apoptosis of cholangiocarcinoma cells via endoplasmic reticulum stress. Oncology letters. 16(3), 3509–3516. doi:10.3892/ol.2018.9131
22. Goldman EH, Chen L, Fu H (2004). Activation of apoptosis signal-regulating kinase 1 by reactive oxygen species through dephosphorylation at serine 967 and 14-3-3 dissociation. The Journal of

biological chemistry. 279(11), 10442–10449. doi:10.1074/jbc.M311129200

23. Bray F, Ferlay J, Soerjomataram I, Siegel RL, Torre LA, Jemal A (2018). Global cancer statistics 2018: GLOBOCAN estimates of incidence and mortality worldwide for 36 cancers in 185 countries. CA: a cancer journal for clinicians. 68(6), 394–424. doi:10.3322/caac.21492
24. Anwanwan D, Singh SK, Singh S, Saikam V, Singh R (2020). Challenges in liver cancer and possible treatment approaches. Biochimica et biophysica acta. Reviews on cancer. 1873(1), 188314. doi:10.1016/j.bbcan.2019.188314
25. Bich Ngoc TT, Hoai Nga NT, My Trinh NT, Thuoc TL, Phuong Thao DT (2020). Elephantopus mollis Kunth extracts induce antiproliferation and apoptosis in human lung cancer and myeloid leukemia cells. Journal of ethnopharmacology. 263, 113222. doi:10.1016/j.jep.2020.113222
26. Yang J, Li ZD, Hou CY, Li ZY, Li Q, Miao SY, Zhang Q, Zhang XY, Zhu XF, Jiang JW (2021). EM-2 inhibited autophagy and promoted G2/M phase arrest and apoptosis by activating the JNK pathway in hepatocellular carcinoma cells. Acta pharmacologica Sinica. 42(7), 1139–1149. doi:10.1038/s41401-020-00564-6
27. Li J, Tang G, Qin W, Yang R, Ma R, Ma B, Wei J, Lv H, Jiang Y (2018). Toxic effects of arsenic trioxide on Echinococcus granulosus protoscoleces through ROS production, and Ca2+-ER stress-dependent apoptosis. Acta biochimica et biophysica Sinica. 50(6), 579–585. doi:10.1093/abbs/gmy041
28. Matsuzawa A, Ichijo H (2001). Molecular mechanisms of the decision between life and death: regulation of apoptosis by apoptosis signal-regulating kinase 1. Journal of biochemistry. 130(1), 1–8. doi:10.1093/oxfordjournals.jbchem.a002947

Figures

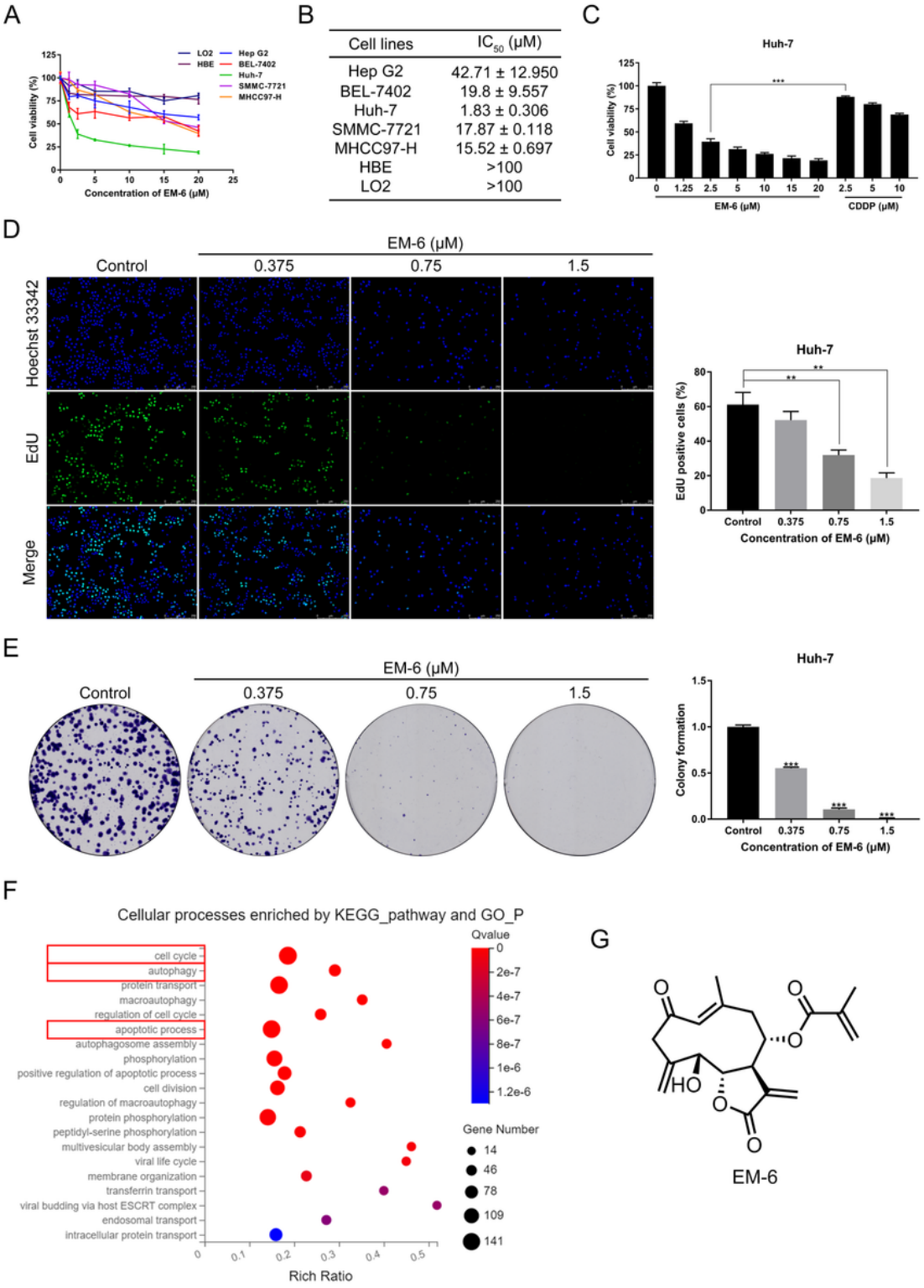

Figure 1

EM-6 inhibited the proliferation of Huh-7 cells.

(A) Several hepatocellular cancer cell lines and normal liver epithelial LO2 and bronchial epithelial HBE cellswere exposed to different concentrations of EM-6 for 48 h, as determined by the MTT assay. The data are presented as the means ± SDs of three independent experiments (**P<0.01, ***P<0.001).(B) The

IC50s for human hepatocellular cancer cell lines and epithelial cells. (C) Huh-7 cells were exposed to different concentrations of EM-6 or CDDP for 48 h, as determined by MTT assay. The data are presented as the means ± SDs of three independent experiments (**P<0.01, ***P<0.001). (D, E) The inhibitory effect of EM-6 on Huh-7 cell proliferation was detected by EdU and colony formation assays. The data are presented as the means ± SDs of three independent experiments (**P<0.01, ***P<0.001). Scale bars: 250 μm. (F) GO function and KEGG enrichment analysis. A Q value ≤ 0.05 indicated a significant difference. (G) The chemical structure of EM-6.

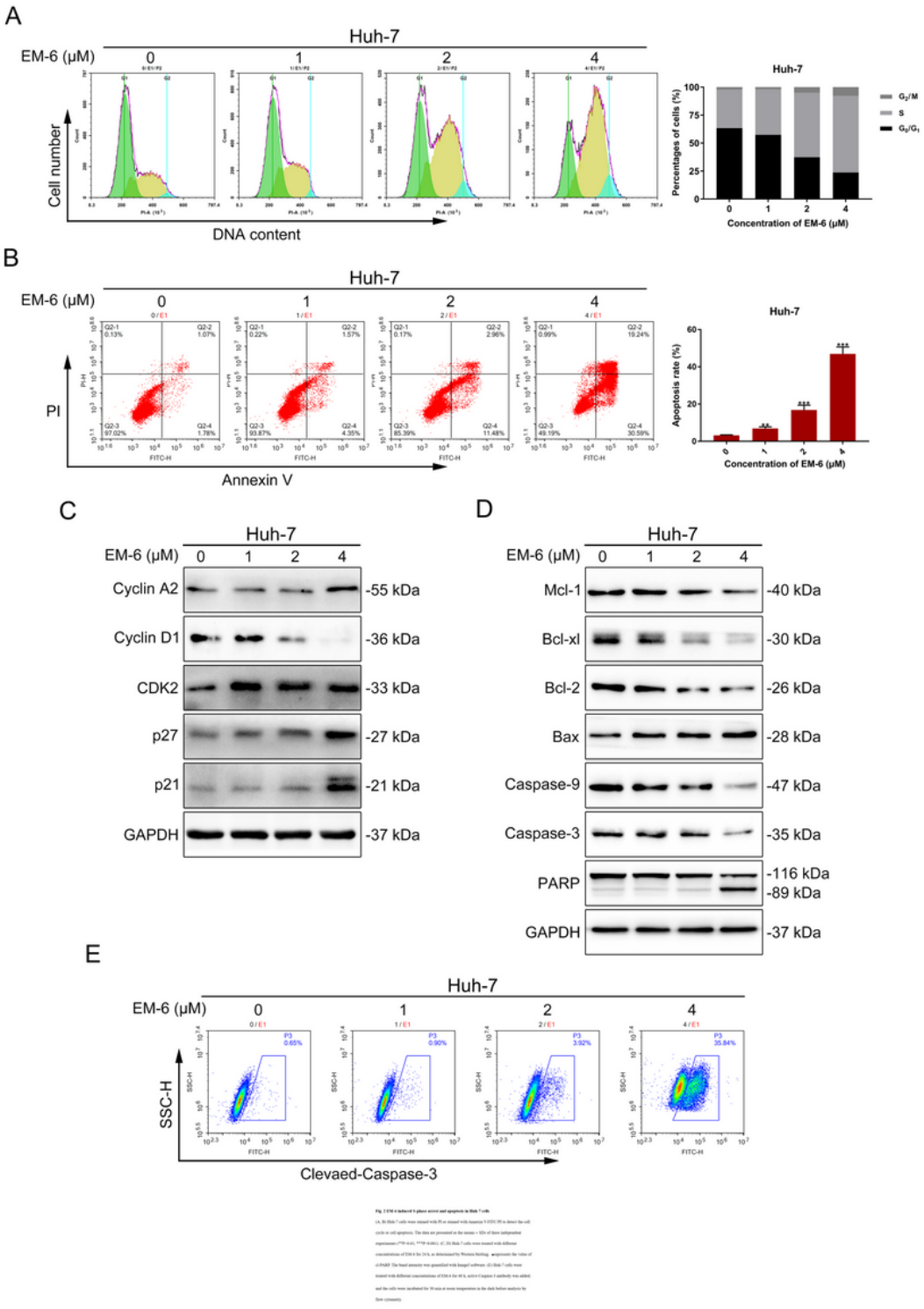

Figure 2

See image above for figure legend.

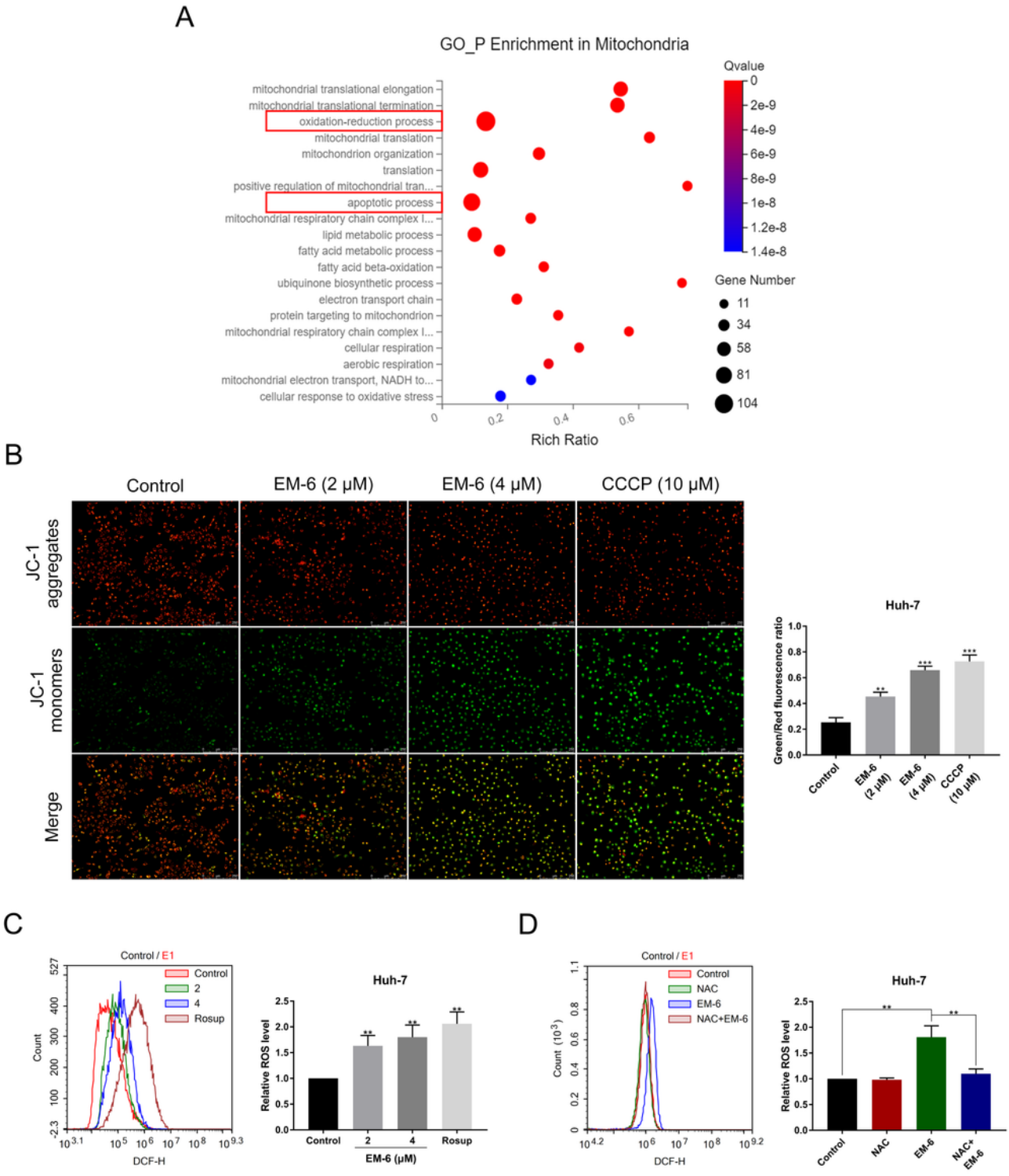

Figure 3

EM-6 induced a decrease in the mitochondrial membrane potential and accumulation of ROS

(A) GO enrichment analysis of biological processes. A Q value≤0.05 indicated a significant difference. (B) Huh-7 cells were treated with different concentrations of EM-6 for 24 h and CCCP (10 μM) as a positive control for 20 min. Cells were stained with the JC-1 probe and imaged via fluorescence microscopy. Scale bars: 250 μm. The data are presented as the means ± SDs of three independent experiments (**P<0.01, ***P<0.001). (C, D) Huh-7 cells were treated with different concentrations of EM-6 for 8 h with or without NAC (5 mM, 1 h) or with Rosup (50 μg/mL) as a positive control for 30 min and then detected by flow cytometry. The data are presented as the means ± SDs of three independent experiments (**P<0.01, ***P<0.001).

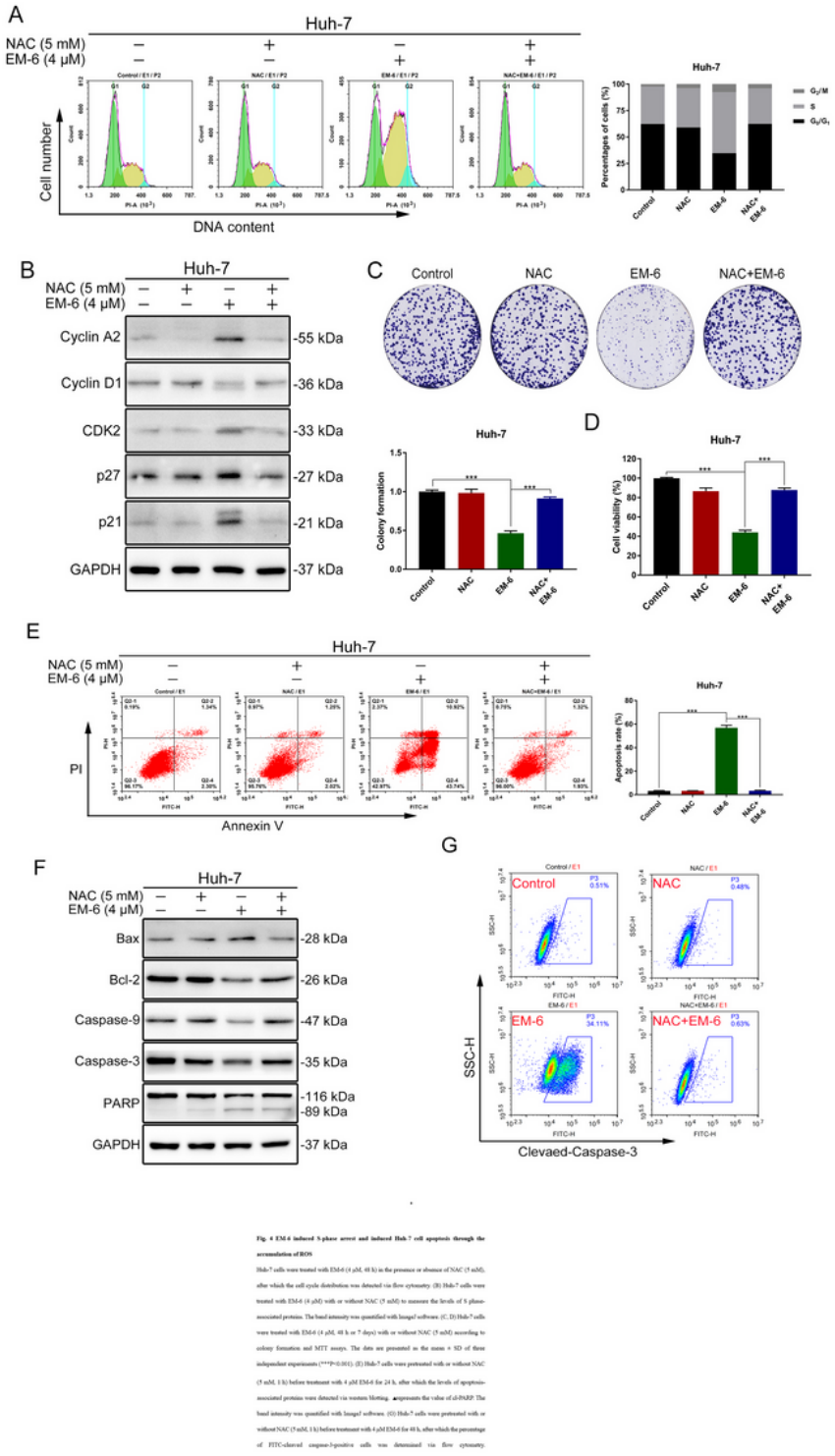

Fig. 4 EM-6 induced S-phase arrest and induced Huh-7 cell apoptosis through the accumulation of ROS

Huh-7 cells were treated with EM-6 (4 μM, 48 h) in the presence or absence of NAC (5 mM), after which the cell cycle distribution was detected via flow cytometry. (B) Huh-7 cells were treated with EM-6 (4 μM) with or without NAC (5 mM) to measure the levels of S phase-associated proteins. The band intensity was quantified with ImageJ software. (C, D) Huh-7 cells were treated with EM-6 (4 μM, 48 h or 7 days) with or without NAC (5 mM) according to colony formation and MTT assays. The data are presented as the mean ± SD of three independent experiments (****P<0.001). (E) Huh-7 cells were pretreated with or without NAC (5 mM, 1 h) before treatment with 4 μM EM-6 for 24 h, after which the levels of apoptosis-associated proteins were detected via western blotting. **a** represents the value of cl-PARP. The band intensity was quantified with ImageJ software. (G) Huh-7 cells were pretreated with or without NAC (5 mM, 1 h) before treatment with 4 μM EM-6 for 48 h, after which the percentage of FITC-cleaved caspase-3-positive cells was determined via flow cytometry.

Figure 4

See image above for figure legend.

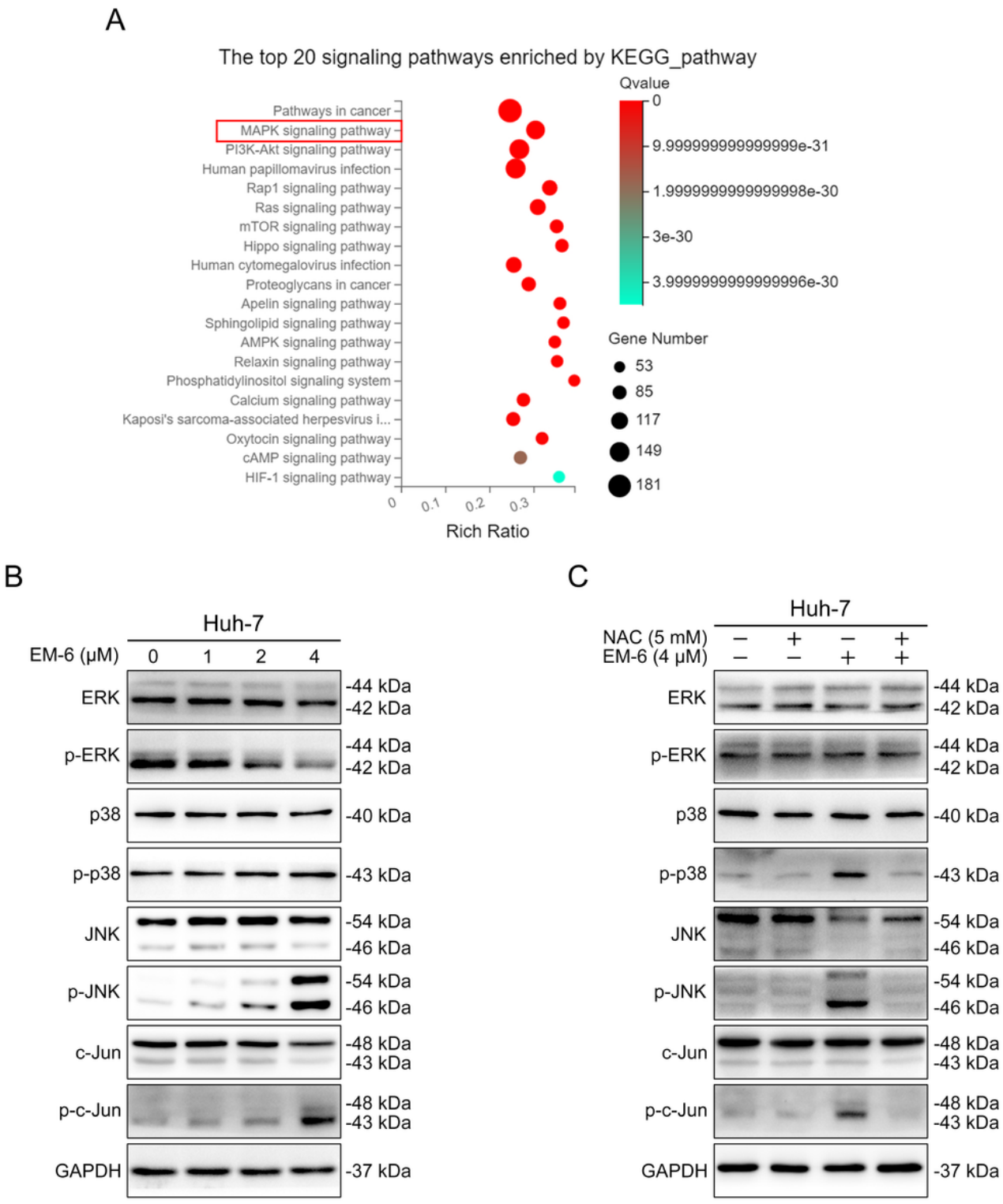

Figure 5

EM-6 activated the MAPK signaling pathway via ROS

(A) KEGG pathway enrichment analysis was performed for the RNA-seq data. A Q value ≤ 0.05 indicated a significant difference. (B, C) Huh-7 cells were pretreated with or without NAC (5 mM, 1 h) before

treatment with 4 μM EM-6 for 24 h. Western blotting was performed to detect MAPK family proteins. The band intensity was quantified with ImageJ software.

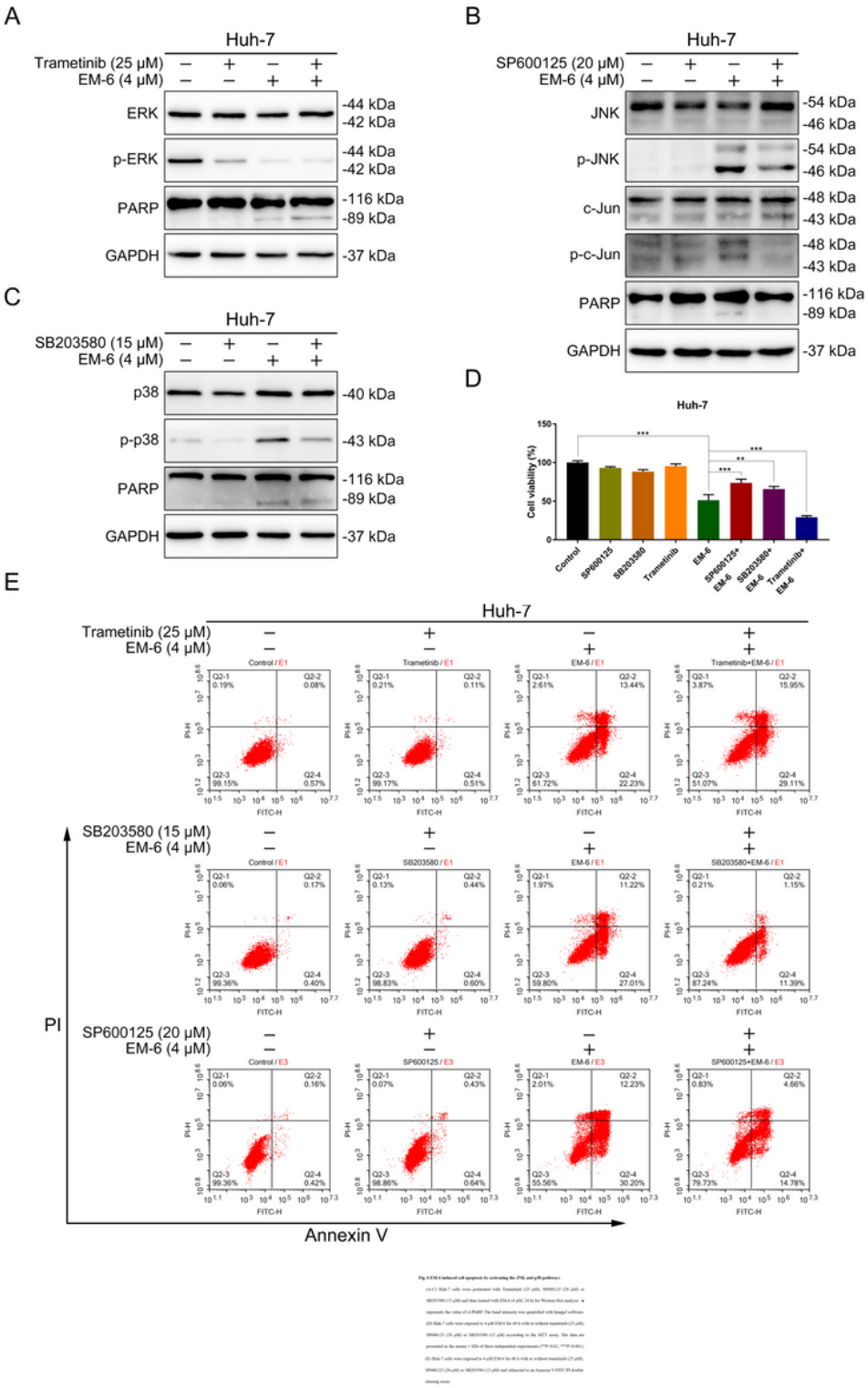

Figure 6

See image above for figure legend.

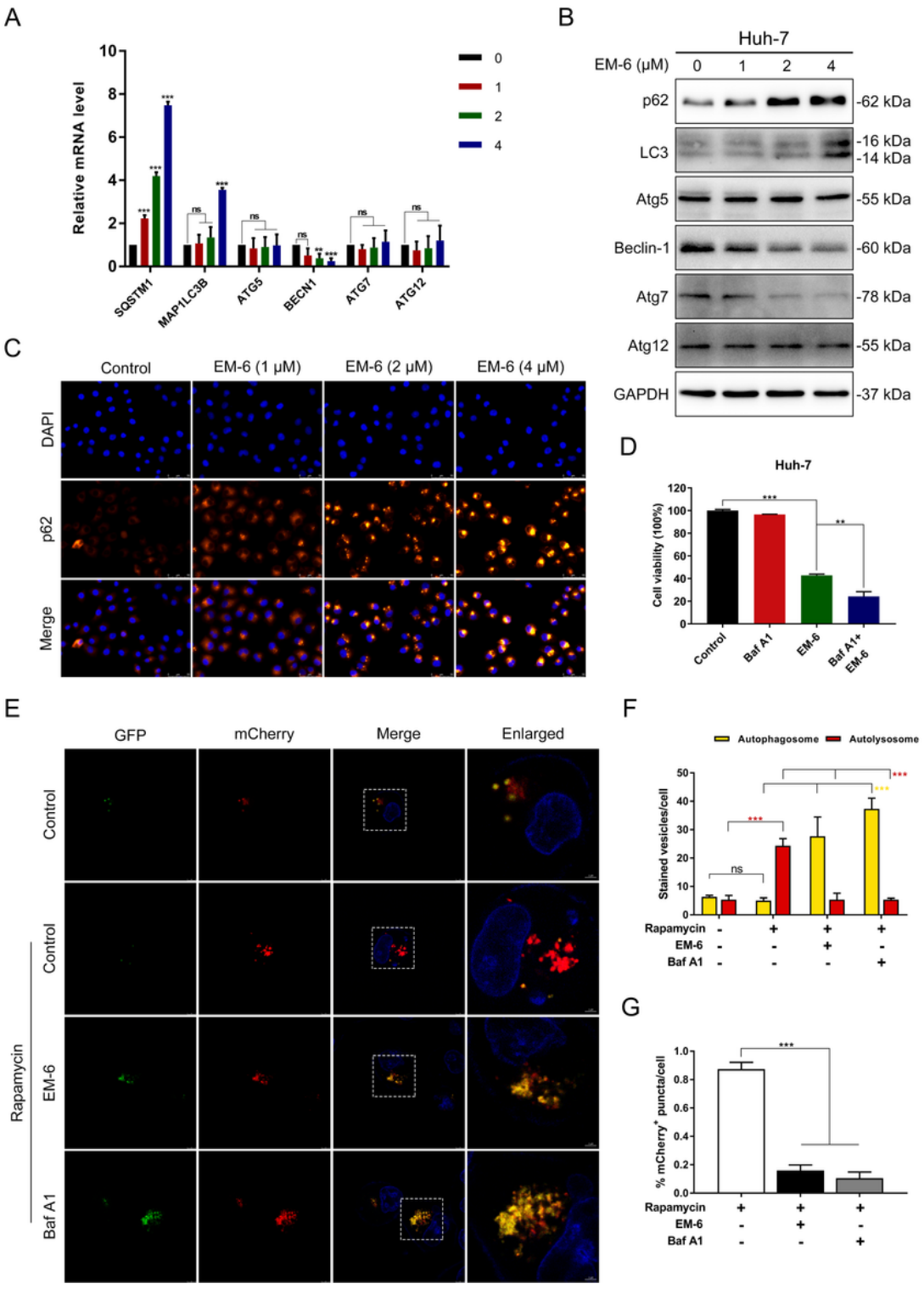

Figure 7

EM-6 blocked autophagic flux in Huh-7 cells

(A) qRT–PCR was performed to detect the mRNA levels of genes associated with autophagy. The data are presented as the mean ± SD of three independent experiments(***P<0.001; ns, not significant).(B) Huh-7 cells were exposed to different concentrations of EM-6 for 24 h, as determined by Western blotting.

The band intensity was quantified with ImageJ software. (C) Huh-7 cells were exposed to different concentrations of EM-6 for 24 h with an anti-p62 antibody, as determined by immunofluorescence. Scale bars: 50 μm. (D) Huh-7 cells were treated with 4 μM EM-6 for 48 h with or without Baf A1 (100 nm, 8 h) according to the results of the MTT assay. The data are presented as the mean ± SD of three independent experiments (**P<0.01, ***P<0.001). (E) Huh-7 cells transfected with GFP-mCherry-LC3 lentivirus were incubated with rapamycin (100 nm, 4 h) and treated with EM-6 (4 μM; 24 h) or BafA1 (100 nM; 8 h). Scale bars: 5 μm. (F, G) Quantification of autophagosomes (yellow fluorescent dots) and autolysosomes (red fluorescent dots) in Huh-7 cells. The data are presented as the mean ± SD of three independent experiments(***P<0.001; ns, not significant).

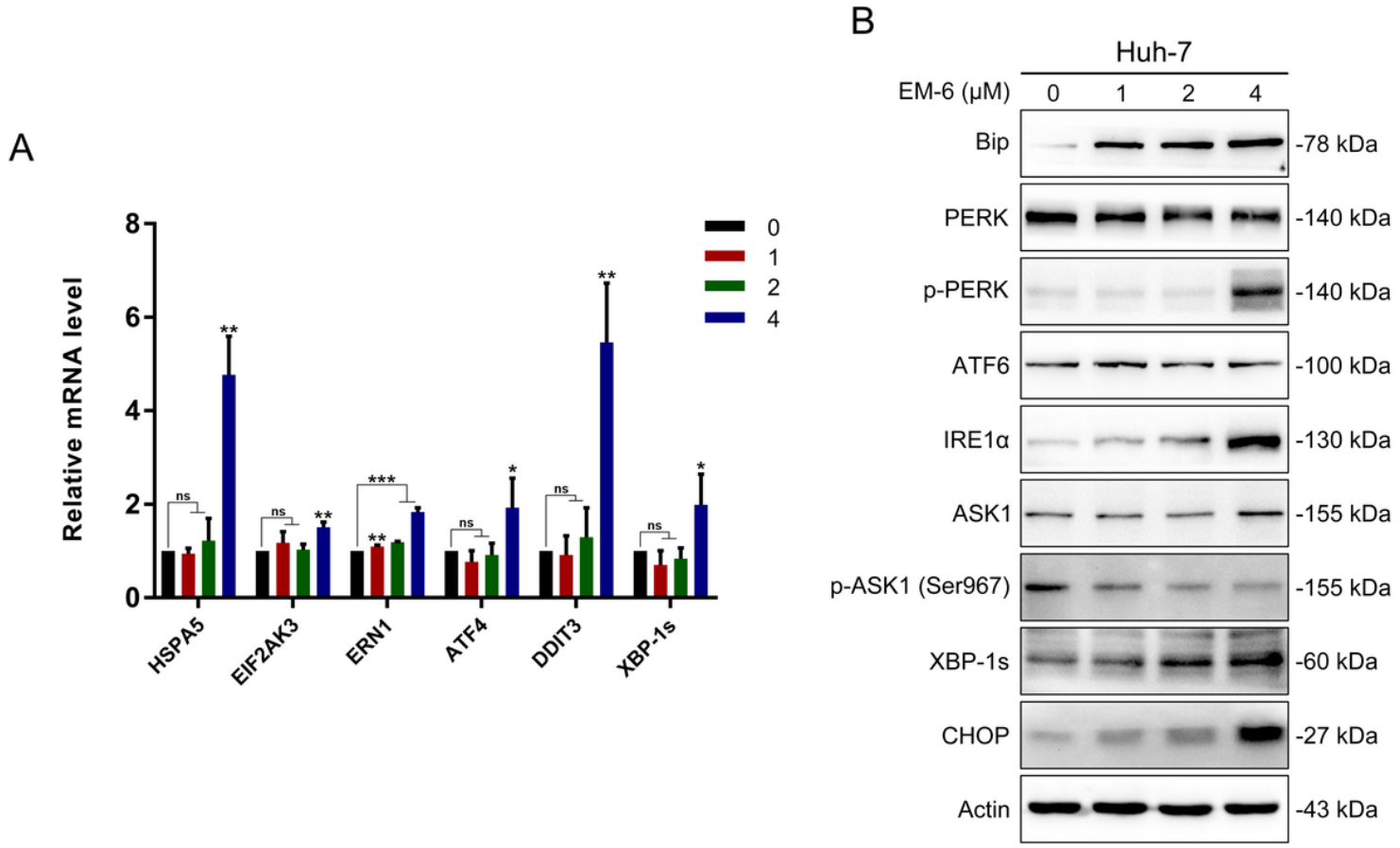

Figure 8

EM-6 activated ER stress-associated apoptosis

(A) Huh-7 cells were exposed to different concentrations of EM-6 for 24 h. qRT—PCR was performed to detect the mRNA levels of genes associated with ER stress. (B) Huh-7 cells were exposed to different concentrations of EM-6 for 24 h, and the expression levels of proteins associated with endoplasmic reticulum stress were analyzed via Western blotting. The relative expression levels of the ER stress-related proteins in Huh-7 cells were quantified via ImageJ software.

Supplementary Files

This is a list of supplementary files associated with this preprint. Click to download.

- GraphicalAbstract.tif